AAAS
Research
Volume 2020, Article ID 7043124, 11 pages
https://doi.org/10.34133/2020/7043124

Research
A SCIENCE PARTNER JOURNAL

Research Article

Semi-Quantitatively Designing Two-Photon High-Performance Fluorescent Probes for Glutathione S-Transferases

Xue-Xiang Zhang,[1] **Huan Qi**,[2] **Mei-Heng Lu**,[1] **Song-Qiu Yang**,[1] **Peng Li**,[3] **Hai-long Piao**,[2] **and Ke-Li Han**[1,3]

[1]*State Key Laboratory of Molecular Reaction Dynamics, Dalian Institute of Chemical Physics, Chinese Academy of Sciences, Dalian 116023, China*
[2]*CAS Key Laboratory of Separation Science for Analytical Chemistry, Dalian Institute of Chemical Physics, Chinese Academy of Sciences, Dalian 116023, China*
[3]*Institute of Molecular Sciences and Engineering, Shandong University, Qingdao 266237, China*

Correspondence should be addressed to Hai-long Piao; hpiao@dicp.ac.cn and Ke-Li Han; klhan@dicp.ac.cn

Received 21 December 2019; Accepted 18 February 2020; Published 21 March 2020

Copyright © 2020 Xue-Xiang Zhang et al. Exclusive Licensee Science and Technology Review Publishing House. Distributed under a Creative Commons Attribution License (CC BY 4.0).

Glutathione S-transferases (GSTs), detoxification enzymes that catalyze the addition of glutathione (GSH) to diverse electrophilic molecules, are often overexpressed in various tumor cells. While fluorescent probes for GSTs have often adopted the 2,4-dinitrobenzenesulfonyl (DNs) group as the receptor unit, they usually suffer from considerable background reaction noise with GSH due to excessive electron deficiency. However, weakening this reactivity is generally accompanied by loss of sensitivity for GSTs, and therefore, finely turning down the reactivity while maintaining certain sensitivity is critical for developing a practical probe. Here, we report a rational semiquantitative strategy for designing such a practical two-photon probe by introducing a parameter adopted from the conceptual density functional theory (CDFT), the local electrophilicity ω_k, to characterize this reactivity. As expected, kinetic studies established ω_k as efficient to predict the reactivity with GSH, and probe NI3 showing the best performance was successfully applied to detecting GST activities in live cells and tissue sections with high sensitivity and signal-to-noise ratio. Photoinduced electron transfer of naphthalimide-based probes, captured by femtosecond transient absorption for the first time and unraveled by theoretical calculations, also contributes to the negligible background noise.

1. Introduction

Glutathione S-transferases (GSTs, EC 2.5.1.18), mainly known as phase II detoxifying enzymes [1], are a family of dimeric enzymes that catalyze the nucleophilic attack of the sulfhydryl of glutathione (GSH) on an electrophilic center of diverse substrates of endogenous or exogenous origin [2]. The expression level of GSTs plays a crucial role in determining the susceptibility to cancer chemotherapy [3]. Among varieties of GST isoenzymes, alpha (GSTA), mu (GSTM), and pi (GSTP) are frequently found overexpressed in various tumor cell lines, particularly in anticancer drug-resistant ones [4–8]. Hence, sensitively and specifically monitoring GST activities in biological systems without background noise, namely, false-positive error usually introduced by GSH, is urgently needed.

Recently, small-molecule fluorescent probes have been rapidly emerging as a powerful tool for enzyme detection in biological samples by virtue of their fast analysis, higher sensitivity, minimal perturbation to living systems, and real-time detection capabilities [9–13]. Indeed, several such probes have been developed for sensitive detection of GST activities with representatives being DNAT-Me [14], DNs-CV [15], and 3,4-DNADCF [16]. However, these probes exhibit either high nonenzymatic background noise or narrow isoenzyme selectivity. Specifically, while the 2,4-dinitrobenzenesulfonyl (DNs) group has often been employed as a receptor unit for GST probes [15, 17], those probes for thiols such as GSH and cysteine mostly just adopt the same group [18–20], demonstrating the nonnegligible background noise due to the nonenzymatic reaction between GSH and this very group. Given the considerable concentration of GSH (*ca.* 1–10 mM)

in mammalian cells, interferences from this GSH noise with GST detection should not be ignored. However, a probe with higher sensitivity for GSTs is usually accompanied by a higher nonenzymatic background noise due to its chemical reactivity with GSH, which implies that alleviating this noise is also at the expense of sensitivity. Therefore, finely tuning the reactivity with GSH is critical for designing a practical probe for GSTs with both specificity and sensitivity.

It is conceivable that an effective parameter characterizing the reactivity of one GST probe with GSH should be conducive to molecular design for the sake of subtle tuning. It is well documented that GST catalyzes the nucleophilic attack of GSH on the electrophilic center of its substrate via nucleophilic aromatic substitution (S_NAr) reaction mechanism [1, 21], so what is desired should be a parameter reflecting the effective electrophilicity of a probe. Therefore, we turned to the local electrophilicity ω_k [22], a concept quoted from conceptual density functional theory (CDFT), which has been extensively employed to investigate Diels-Alder reactions [23–26]. As shown in Equation (1), ω_k is equal to the arithmetic product of the global electrophilicity ω [27] and the electrophilic Parr function P_k^+ [22], the latter one being an approximation of the condensed Fukui function f_k^+, which characterizes the regioselectivity. With GSH generally accepted as a so-called soft nucleophile and nitrobenzene derivative a soft electrophile [28], it is reasonable to use this parameter to describe the reactivity [29, 30].

$$\omega_k = \omega \cdot P_k^+. \quad (1)$$

Here, we present the first rational semiquantitative strategy for designing practical two-photon fluorescent probes for GSTs with both high sensitivity and negligible background noise. First, based on the S_NAr reaction mechanism, we established that the electrophilic Parr function P_k^+ could characterize the regioselectivity of a probe, and therefore, the local electrophilicity ω_k can be used to represent and predict relative chemical reactivity of different probes. Hence, a series of probe candidates were designed and screened out according to their ω_k values, which were available by quantum chemical calculations. These probes were synthesized and evaluated in terms of sensitivity and signal-to-noise (S/N) ratio, after which **NI3** was selected and successfully applied to the imaging of GST activities in live cells and tissue sections with high sensitivity and S/N ratio. Furthermore, femtosecond transient absorption spectra and time-dependent density functional theory (TD-DFT) calculations revealed the photoinduced electron transfer (PET) mechanism of fluorescence quenching, which also contributed to the considerably low background noise.

2. Results

2.1. Designing and Screening of the Probe Candidates. As stated earlier, the DNs group has often been employed as a receptor unit for GST detection probes; we thus started to design our first two-photon fluorescent probe candidate **NI1** by introducing the DNs group to the ring of 4-hydroxyl-*N*-butyl-1,8-naphthalimide (**NI**), a well-known fluorophore with two-photon absorptivity [31, 32]. Initially, to examine whether the calculation method introduced here is rational, the electronic spin density distribution and the atomic spin population (namely, the P_k^+ values) of the anion radical of **NI1** were calculated. The α-carbon of the arylsulfonyl group showed the maximum spin density and P_k^+ (Figure 1), indicating the most electrophilic center lies on this very carbon, which is to be attacked by GSH, in accord with the regioselectivity revealed by previous experiments [15, 17]. This result indicates that it is the electronic aspects related to electrophilicity rather than other factors such as the leaving ability of the nucleofuge related to nuclear displacement [33, 34] that dominate the regioselectivity herein. Confirming P_k^+'s ability to reproduce the real regioselectivity led to the conclusion that the effective reactivity of a probe with GSH could be characterized by the local electrophilicity ω_k of the α-carbon (refer to Equation (1)). It can be envisaged that by altering substitution situations on the nitrobenzene ring and comparing ω_k of resultant probe candidates, some superior probes will be preliminarily screened out with the criterion: the ω_k of a practical probe should be modestly lower than that of **NI1**.

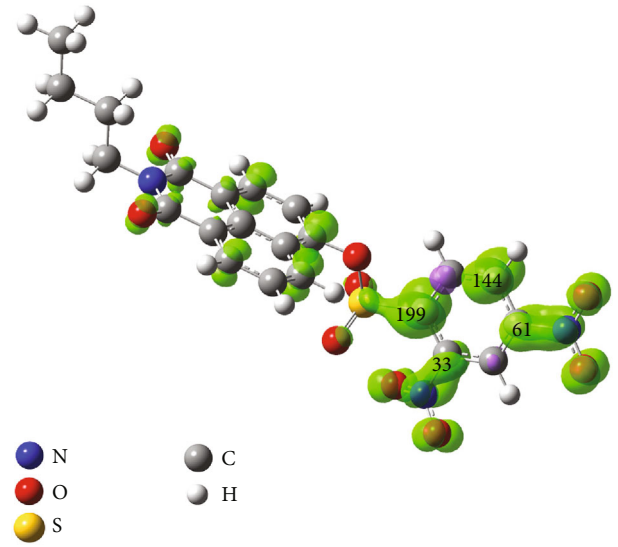


Figure 1: Spin density distribution of the anion radical of **NI1**. Respective positive P_k^+ value (amplified by a factor of 1,000) of the carbon atoms in the nitrobenzene ring is marked, with positive and negative spin density colored by green and purple, respectively. Negative spin density or P_k^+ values are herein regarded as meaningless [35, 36]. Isodensity value = 0.002.

Considering the DNs group is a much too sensitive receptor unit, five approaches were put forward (Figure 2): (1) replace the second nitro group, the one *para* to the α-carbon, with less electron-withdrawing groups to give **NI2** and **NI3**; (2) add an electron-donating group to the position *meta* to the α-carbon to give **NI4** and **NI5**; (3) simply shift the second nitro group to other positions to give **NI11**, **NI12**, and **NI13**; (4) first, shift the second nitro group to the other position *ortho* to the α-carbon, and then, replace it with less electron-withdrawing groups to give **NI14** and **NI15**; and

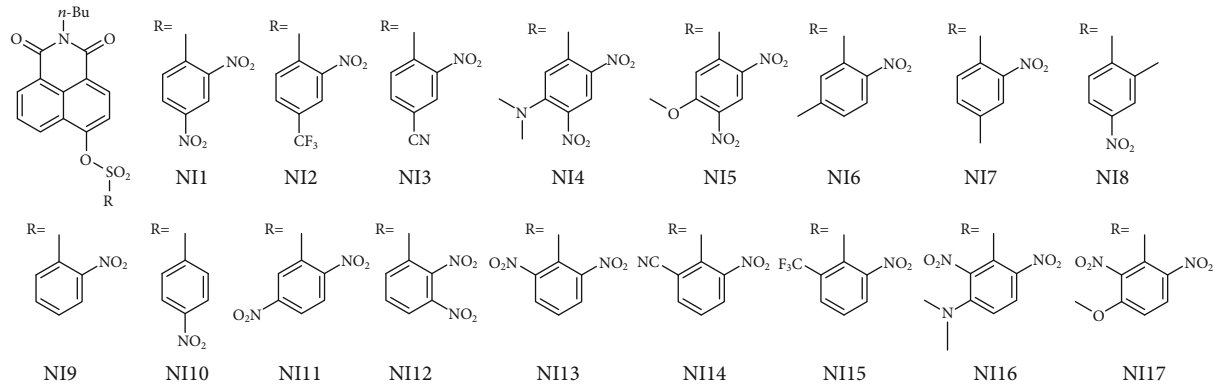


Figure 2: Chemical structures of the probe candidates.

(5) first, shift the second nitro group to the other position *ortho* to the α-carbon, and then, add an electron-donating group to the position *meta* to the α-carbon to give **NI16** and **NI17**. Subsequently, these compounds were evaluated in terms of spin density distribution, P_k^+ and ω_k values, and the results showed that all probe candidates except those in the third approach displayed a valid regioselectivity and reasonably lower ω_k values with **NI5**, **NI3**, and **NI14** among the most moderate ones, suggestive of their potential as practical probes (Figure S1 and Table S1). It should be noted that similar ω_k values appear in **NI1** and **NI13**, **NI3** and **NI14**, **NI2** and **NI15**, or **NI4** and **NI16**, respectively, indicating that there is no significant difference in the electron-withdrawing group's locating *para* or *ortho* to the α-carbon, which is in line with the chemical intuition. As for **NI11** and **NI12**, the most electrophilic center lies on the alternative β-carbon rather than on the α-carbon (Figure S1), indicative of their inappropriateness as GST detection probes. Actually, one tries synthesizing **NI11** but only to find that apart from the fluorine atom, one nitro group was substituted competitively and comparably by the sulfonic group just via the S_NAr reaction mechanism (Figure S2; refer to the synthesis section below and in Supplementary Materials; for more evidence for the applications of P_k^+ and ω_k, refer to Figures S3–4 and Tables S2–3).

Taking both the above results and the practical complexity of chemosynthesis into account, we determined to synthesize **NI5**, **NI3**, **NI4**, and **NI2**, with **NI1** also prepared as a representative for oversensitive probes. In addition, since this is the first time ω_k has been introduced for designing GST detection probes, less sensitive receptor units which emerged in the previous literature [3, 15] were also adopted to give **NI6**, **NI7**, **NI8**, **NI9**, and **NI10** to reveal the relationship between chemical structures and sensitivities in more detail. Notably, although they share the same regioselectivity as that of **NI1** (Figure S1), their ω_k values are somewhat too minor relative to the latter's (Table S1).

2.2. Synthesis and In Vitro Evaluation of the Probe Candidates. To synthesize these probe candidates, a facile three-step procedure was adopted from starting materials either commercially available or conveniently synthesized (refer to Supplementary Materials). In essence, a sulfonic group was introduced by treating the appropriate nitrofluorobenzene derivative with sodium sulfite in a solvent mixture of water and ethanol, the reaction mechanism of which happens to be S_NAr as well, followed by chlorination with thionyl chloride or phosphoryl chloride to give the receptor unit, which was then readily attached to the hydroxyl of **NI** to prepare the final compound. It is worth mentioning that this synthetic route circumvents the conventional method calling for poisonous gas SO_2. Compounds **NI1**–**NI10** and relevant intermediate products were fully characterized using NMR spectroscopy (Figures S20–S57) and mass spectrometry.

With these probe candidates in hand, we investigated whether they were amenable to GST detection *in vitro*. On the whole, upon encounter with GSTs from the equine liver, all these probe candidates gained a drastic enhancement in fluorescence intensity from a virtually nonluminescence state, despite their different S/N ratios (Figure S5). For instance, **NI9** showed beyond 35-fold fluorescence increase at 560 nm in less than 30 minutes (Figure 3(a)). To confirm the probe was lightened by no other than GST activities, a full set of control experiments were conducted. As shown in Figure 3(b), hardly any fluorescence was triggered without either of GST and GSH or both, using deactivated GSTs or replacing the GSH with other sulphur-bearing analogues, namely, oxidized glutathione, *N*-acetylcysteine, *L*-cysteine, and *L*-homocysteine. In addition, if ethacrynic acid (EA), a well-known inhibitor for various GSTs [37], was added 30 min prior to GSH and **NI9**, the rising of fluorescence was substantially suppressed (Figure 3(b)). These results demonstrate that GST and GSH are both indispensable to the fluorescence enhancement. Further, with both of the resultant organic products being captured and tracked, the UPLC-MS analysis (Figure S6) as well as the spectra comparison (Figure S7) provided a more explicit and solid evidence that the detection mechanism is exactly the one illustrated in Figure 3(c). As designed, under the catalysis of GST, the attack of GSH on the α-carbon releases glutathione conjugate, SO_2, and **NI**, enabling the detection of GST activities.

Although every single probe did display measurable response towards GSTs, they differed greatly from one

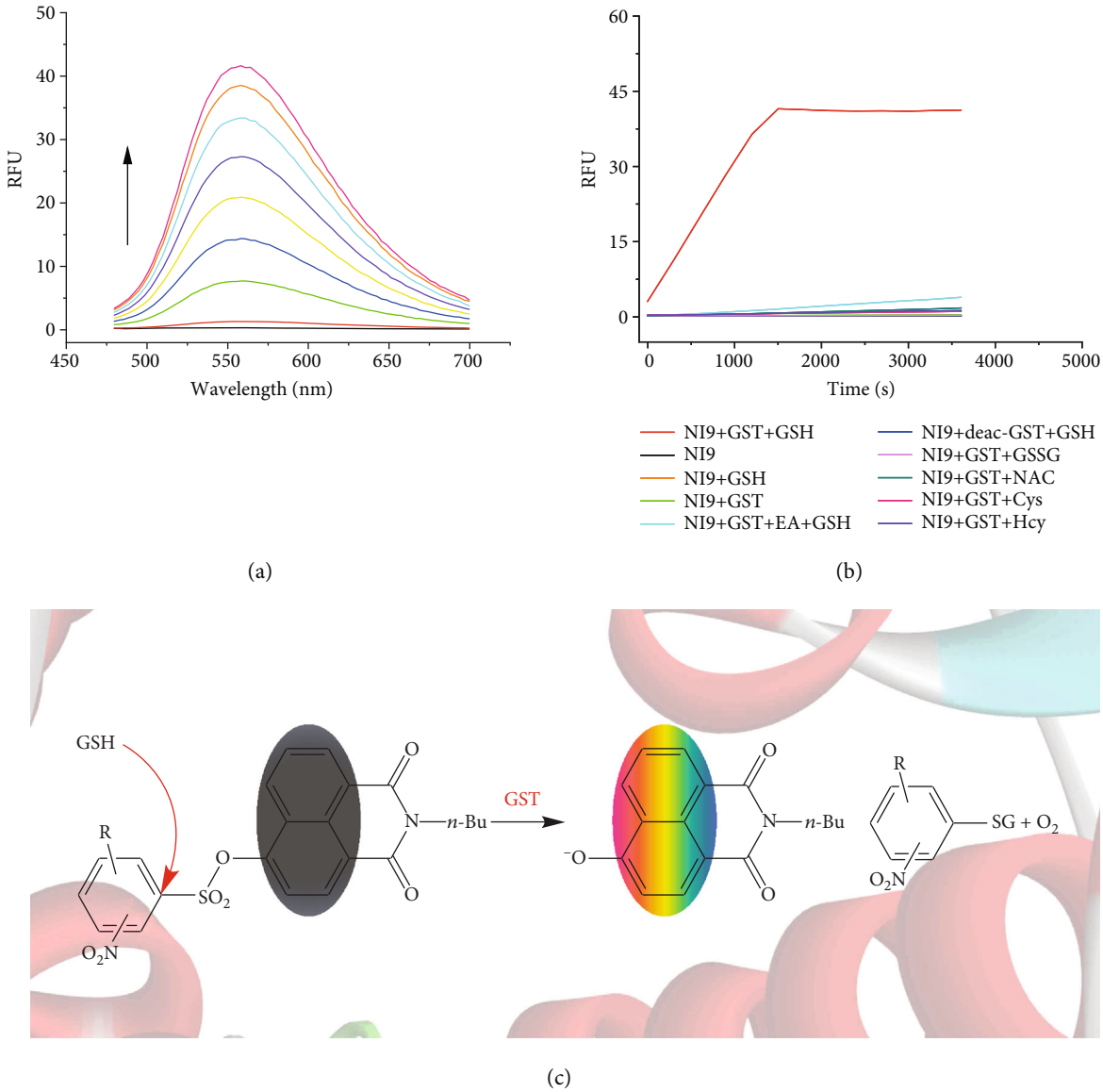


FIGURE 3: *In vitro* GST detection with NI9 and the detection mechanism for **NI**-series probes. (a) Time-dependent fluorescence spectra of **NI9** (20 μM) in HEPES buffer (20 mM, 0.5% DMSO, pH 7.4) upon addition of GSTs (12.5 μg/mL) over the course of 25 min at 37°C in the presence of GSH (2 mM). λ_{ex} = 445 nm. (b) A full set of control experiments on examining the cause of fluorescence enhancement. EA = ethacrynic acid (GSTs were preincubated with 200 μM EA for 30 min before addition of GSH and **NI9** sequentially); deac-GST = deactivated GSTs (12.5 μg/mL) by pretreatment at 100°C for 10 min; GSSG = oxidized glutathione (2 mM); NAC = *N*-acetylcysteine (2 mM); Cys = *L*-cysteine (2 mM); Hcy = *L*-homocysteine (2 mM). $\lambda_{ex/em}$ = 445/560 nm. (c) Schematic for the proposed GST activity detection mechanism of **NI**-series probes.

another in terms of sensitivity and nonenzymatic noise. For example, with rapid response to either GSTs or GSH, **NI1** is regarded as an oversensitive probe, whereas **NI6** belongs to undersensitive probes due to slow response towards GSTs, along with no background noise at all (Figures S5a,f and S8). In order to inspect the relationship between chemical structures of the probes and their performances quantitatively, an elaborate kinetic study on both nonenzymatic and enzymatic reactions was implemented, and the kinetic parameters were plotted as the function of ω_k values of the α-carbon (Figure 4 and Tables S4–S6). With all the probes whose nonenzymatic reactions with GSH are detectable falling into the quasilinear plot of ln k_{nonc} and ln ω_k (the goodness of fit R^2 = 0.991), the local electrophilicity ω_k proved itself an excellent parameter to describe the S_NAr reactivity with GSH, namely, the nonenzymatic noise for GST detection. Remarkably, the order of k_{nonc} for different probes (**NI2**<**NI4**<**NI3**<**NI5**<**NI1**) agrees quite well with the order of fluorescence rising rate in preceding nonenzymatic tests (Figure S8b), thus corroborating the conclusions drawn here. To our knowledge, this is the first time the

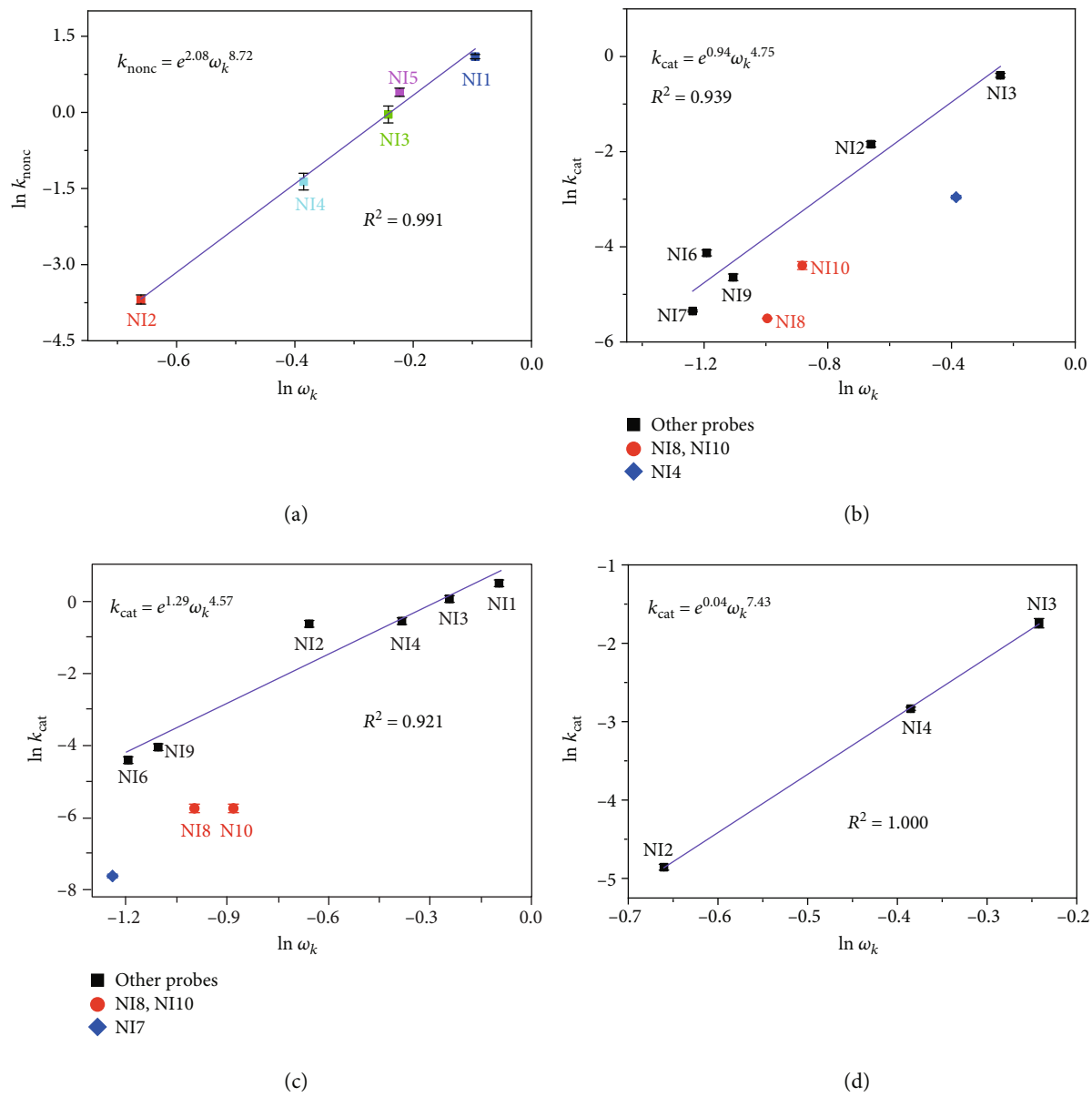


Figure 4: Structure-activity relationships between nonenzymatic or enzymatic kinetic parameters and the local electrophilicity ω_k of the α-carbon. (a) Regarding the second-order rate constant k_{nonc} of the nonenzymatic reaction between GSH and probes. Data for other probes are unavailable due to extremely low reactivity. (b–d) Regarding the catalytic constant k_{cat} of (b) GSTA1-1, (c) GSTM1-1, and (d) GSTP1-1, respectively, towards different probes. Linear fittings were based on mean values. Error bars represent SD.

nonenzymatic noises of probes for GST detection have been depicted and predicted by a single parameter (see Figure S9 for more evidence). Furthermore, to some extent, this parameter can also reflect the probe's sensitivity to GSTs (Figures 4(b)–4(d)). Remarkably, the data of **NI8** and **NI10** deviate from the description by ω_k, demonstrating the o-NO_2 is indispensable to GST catalysis, in agreement with the previous literature [1, 15]. In general, a smaller ω_k means a lower background noise and yet probably a lower sensitivity meanwhile. Then, to what extent do these two aspects depend on the chemical structure, namely, ω_k?

Notably, the preexponential factor (2.08) and exponential term (8.72) of the fitting formula for the nonenzymatic reaction are both larger than the ones for enzymatic reactions (0.94 and 4.75 for GSTA1-1; 1.29 and 4.57 for GSTM1-1; and 0.04 and 7.43 for GSTP1-1), respectively (Figure 4), implying that improving the sensitivity (here depicted by k_{cat}) by enlarging the ω_k would be monotonically accompanied by the loss of S/N ratio (here depicted by k_{cat}/k_{nonc}), in good agreement with preceding results (Figures S5 and S8). Thus, there is a trade-off between sensitivity and S/N ratio, and reaching a balance point between them was critical for a superb probe. Fortunately, the relationships above can also be reviewed from the other side: starting from an oversensitive probe such as **NI1**, a tiny decrease of ω_k would probably afford a drastic reduction in nonenzymatic

noise while leaving the sensitivity almost unchanged (*cf.***NI3** and **NI1** in Figures 4(a) and 4(c); see also Figure S8b), thus obtaining a probe with both high sensitivity and high S/N ratio, self-supporting the design strategy here quantitatively. Therefore, it is unsurprising that after an overall consideration of sensitivity, S/N ratio, and broad isoenzyme selectivity (Table S7), **NI3**, one of the two probes whose ω_k are modestly lower than that of **NI1** (Table S1), was found to be the best one. It was thus used for more practical and rigorous applications such as bioimaging in the next section.

2.3. Fluorescence Imaging of Live Cells and Tissue Sections. It is often desirable to be able to detect very low levels of enzymatic activities in live cells, cell extracts, or tissues. Hence, **NI3** was examined whether it was capable of reporting GST activities by cellular fluorescence imaging. First, HepG2 was selected as an appropriate cell line for GST monitoring according to the Western blotting results (Figure S10). Incubation with 20 μM **NI3** in HEPES buffer (pH 7.4) for just one minute could afford a discernible fluorescence image derived from a completely dark one when no probe was added, and then, the cells gradually became brighter in the following *ca.* 30 min (Figure S11 and Video 1), demonstrating the probe was ignited by the intracellular substances. To ascertain the fluorescence arose from GST activities, cells were pretreated with the GST inhibitor EA and the GSH-depleting agent *N*-ethylmaleimide (NEM), respectively, before the addition of **NI3**. The results showed a substantial loss of fluorescence for both cases (Figures 5(a)–5(c)), proving that it was the attack of GSH on the probe by virtue of GST catalysis that lighted the cells up. A similar consequence was obtained from the flow cytometric analysis (Figure 5(d) and Table S8). Furthermore, an analogous assay in cell lysate samples revealed that the fluorescence intensity of cell lysate pretreated with EA was still obviously higher than that of the control group which represented the nonenzymatic reaction of **NI3** with GSH (Figure 5(e)). This finding implies the remaining fluorescence that appeared in cellular imaging or flow cytometry came from the residual GST activities other than the GSH itself (Figures 5(b) and 5(d)) and thus highlights the remarkably high sensitivity and S/N ratio of **NI3**. Actually, the limit of detection (3σ) was calculated to be 3.7 nM. Moreover, to further verify that the nonenzymatic reaction produces little noise, we selected MHCC97L cells as a negative control and HepG2 together with A549 and HeLa cells as positive controls based on the Western blotting results (Figures S10). After being subjected to **NI3** incubation and fluorescence imaging, MHCC97L cells displayed little fluorescence, whereas other cells exhibited strong emission under the same conditions (Figures 5(f)–5(i)). With almost no GST in the MHCC97L cell line and varied GST isoenzymes in each individual positive cell line, this result manifested the probe's specificity for GSTs with negligible nonenzymatic noise again and broad isoenzyme selectivity as well. Incidentally, when incubated with **NI3**, all cells kept a normal and fine morphology during the whole imaging course, indicating its low cytotoxicity and favorable biocompatibility. In addition, to investigate the source of the GST activities, the colocalization experiment was performed and the results showed the fluorescence spread all over the cytoplasm homogeneously rather than focusing on any organelles (Figures S12–S14), consistent with the GSTs' coming from the whole cytosol. Notably, when HepG2 cells were incubated with 20 μM **NI3** or **NI2** for 30 min, respectively, both cellular imaging and flow cytometry tests exhibited a weaker fluorescence for the latter (Figure S15). Additionally, when pretreated with EA and then incubated with **NI1**, HepG2 cells showed almost the same fluorescence intensity as incubated with only **NI1** (Figure S16), highlighting **NI1**'s nonnegligible background noise. All these consequences were in agreement with previous *in vitro* results, demonstrating the local electrophilicity ω_k does affect a probe's effective performances.

With its ability to detect GST activities certified by single-photon confocal fluorescence imaging, we next tested if **NI3** was amenable to two-photon imaging of more complicated biological samples. Initially, identical consequences were obtained by two-photon cell imaging upon irradiation at 810 nm with a femtosecond pulse laser (Figure S17), establishing the probe's capacity for applications based on two-photon microscopy. Subsequently, **NI3** was interrogated as to whether it could afford clear images of tissue sections containing plenty of GSTs. Hence, the tissues of the liver and lung from female BALB/c mice were cut to 100 μm slices with a frozen slicer and then soaked into the HEPES buffer containing 40 μM **NI3** for 1 h before two-photon microimaging. As shown in Figures 6(b) and 6(d), both liver and lung tissues displayed bright fluorescence, albeit with different GST isoenzymes in them [38, 39], whereas completely dark images were acquired in the absence of **NI3** (Figures 6(a) and 6(c)), with the negligible background autofluorescence benefiting from the near-infrared excitation wavelength implied by the two-photon absorptivity of the probe. Furthermore, fluorescence images of the liver tissue sections at different depths were collected in the Z-scan mode (Figure S18 and Video 2), and the results indicate **NI3** is able to realize tissue imaging as deep as *ca.* 100 μm, which enables the 3D reconstruction of the tissue images (Figure S19). To sum up, these results exhibited the excellent two-photon staining and tissue-penetrating capabilities of **NI3**.

2.4. Fluorescence Quenching Mechanism of Intact NI-Series Probes. The establishment of **NI3**'s outstanding performances is unavailable without the low background noise, which is intimately related not only to the appropriate nonenzymatic reactivity but also to the remarkable "off" state of the intact probe. Thus, it is high time to review the fluorescence quenching mechanism. As not merely **NI3** but all the other intact **NI**-series probes showed well-quenched fluorescence (Figure S5), the nitro group was considered to bring about this property, and thus, **NI9** was selected as the representative subjected to the subsequent exploration. We used femtosecond transient absorption (TA) spectroscopy to monitor spectral changes induced by excitation at 370 nm. Almost the moment the

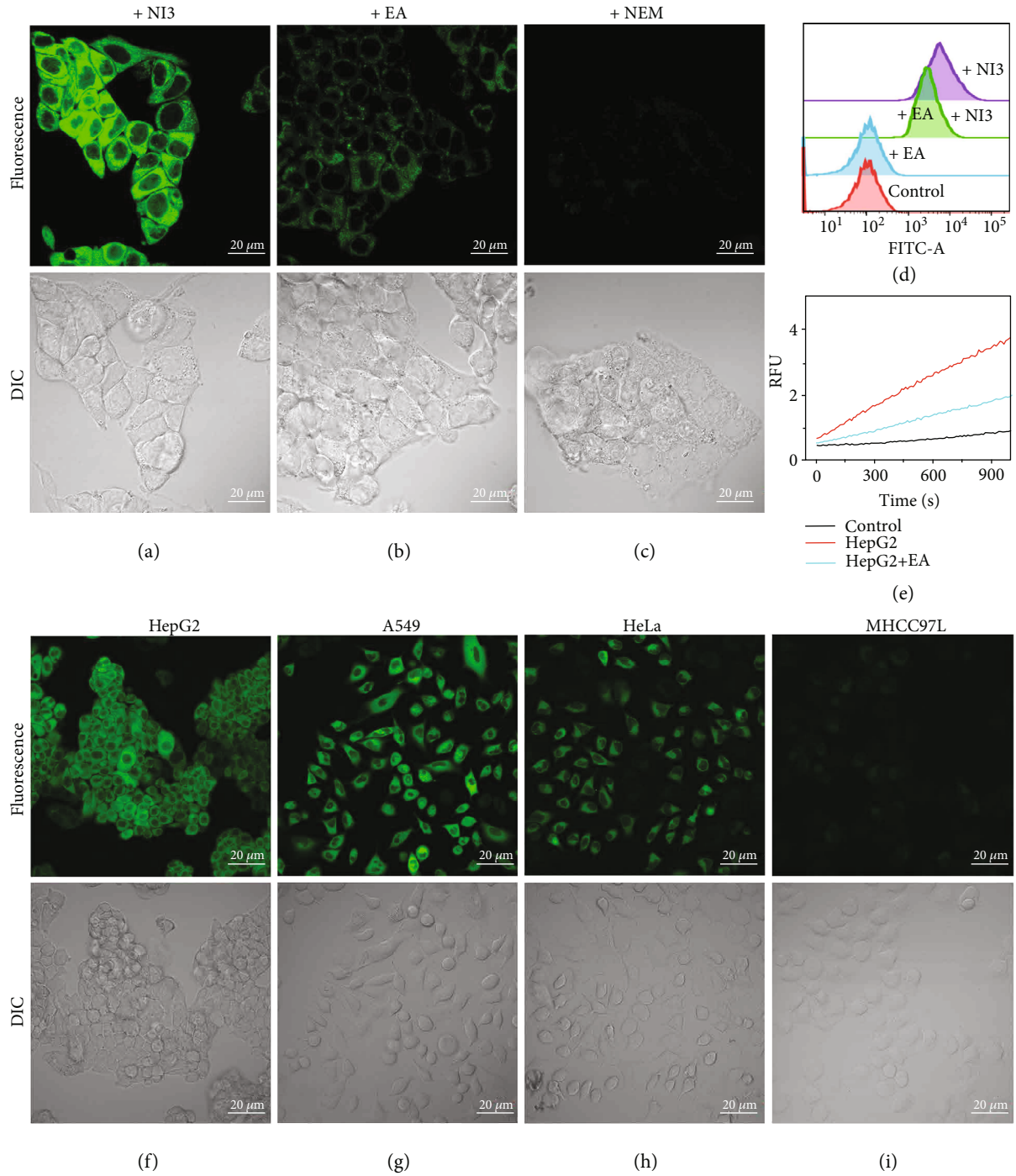


FIGURE 5: (a–c) Single-photon confocal fluorescence imaging of HepG2 cells (a) incubated with 20 μM **NI3**, (b) pretreated with 100 μM EA and then incubated with 20 μM **NI3**, and (c) pretreated with 50 μM NEM and then incubated with 20 μM **NI3** with a 100x objective. λ_{ex} = 458 nm. λ_{em} = 500–600 nm. Scale bar = 20 μm. (d) Flow cytometric analysis of the HepG2 cells. λ_{ex} = 488 nm. λ_{em} = 500–600 nm. (e) Assay of the HepG2 cell lysate using 20 μM **NI3** with 1 mM GSH added in. "Control" means assay without cell lysate. λ_{ex} = 445 nm. λ_{em} = 560 nm. (f–i) Fluorescence images of various cell lines incubated with 20 μM **NI3** for 30 min with a 40x objective. λ_{ex} = 458 nm. λ_{em} = 500–600 nm. Scale bar = 20 μm. Representative images from repeated experiments are shown.

pump light was administrated (<120 fs), a photoinduced absorption band centered at around 484 nm was observed (Figures 7(a) and 7(b)), which is attributed to the formation of the locally excited (LE) state. Subsequently, the absorption of the LE state decreased gradually, accompanied by the emergence of a new absorption band centered at around 429 nm, indicative of the formation of a new state. It is remarkable that the timescales of the decay of the LE state

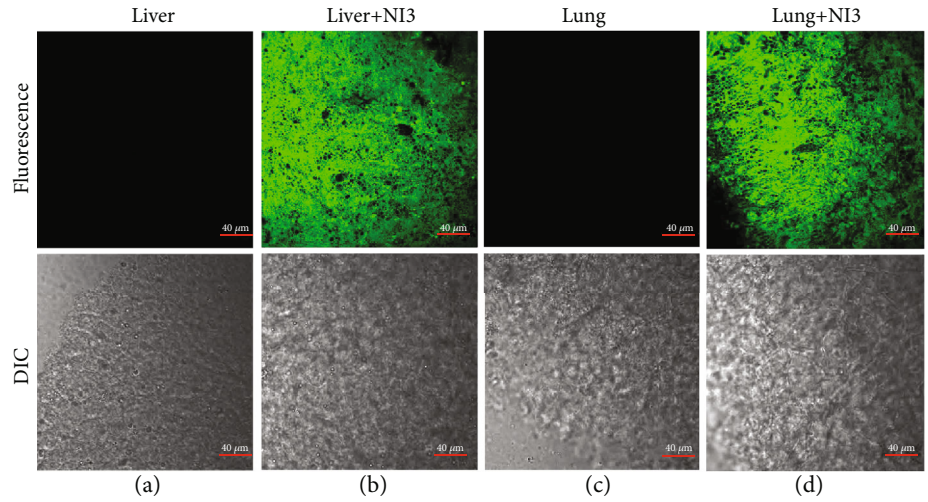


FIGURE 6: Two-photon confocal fluorescence imaging of mouse (a, b) liver and (c, d) lung tissue sections incubated with or without 40 μM **NI3** at a depth of 60 μm with a 60x objective. Scale bar = 40 μm. λ_{ex} = 810 nm. λ_{em} = 520–560 nm.

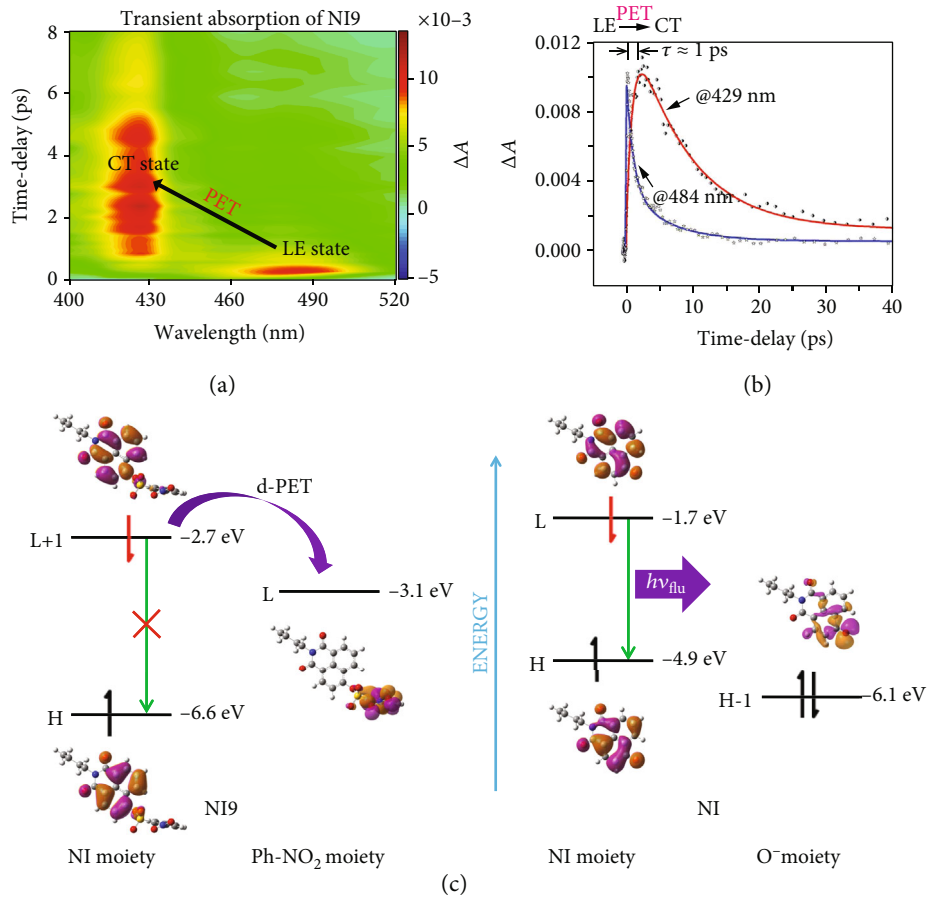


FIGURE 7: Experimental and theoretical studies on the fluorescence quenching mechanism. (a) Pseudocolor femtosecond transient absorption (TA) spectral plot of **NI9** in DMSO. (b) Kinetic traces at different wavelengths following the 370 nm laser pulse excitation and the respective fit with three exponential functions. (c) TD-DFT calculations on the electronic transitions of **NI9** and **NI** in DMSO at the B3LYP/aug-cc-pVDZ level.

and the formation of the new state are both 1 ps according to their respective fits, suggesting the new state was derived from the LE state, which caused the fluorescence quenching.

To elucidate this phenomenon and gain more insight, calculations on the electronic transitions of **NI9** and **NI** were implemented based on the TD-DFT method. As shown in

Table S9, for **NI9**, a small oscillator strength of $S_0 \longrightarrow S_1$ transition ($f = 0.009$) suggests a forbidden transition, demonstrating the S_1 state of **NI9** is not accessible directly from the S_0 state. However, it might be populated via internal conversion from the S_2 state, which arises from a considerable oscillator strength of $S_0 \longrightarrow S_2$ transition ($f = 0.382$). This result is corroborated by the agreement between experimental (360 nm) and calculated (356 nm) maximum absorption wavelengths. The $S_0 \longrightarrow S_2$ transition is dominated by the transition of HOMO to LUMO+1, both of which are located on the **NI** moiety, exhibiting a LE characteristic; the $S_0 \longrightarrow S_1$ transition is dominated by the transition of HOMO to LUMO, the latter being located on the nitrobenzene moiety, exhibiting a charge-transfer (CT) characteristic (Figure 7(c), left). Hence, a donor-excited photoinduced electron transfer (d-PET) process occurred from the **NI** moiety to the nitrobenzene moiety upon excitation owing to the driven force derived from the energy (-2.7 and -3.1 eV for LUMO+1 and LUMO, respectively) gap, quenching the fluorescence, and the new state formed in Figures 7(a) and 7(b) corresponds to **NI9**'s S_1 state, a dark state, also known as the CT state. To our knowledge, this is the first time the actual PET process of **NI**-based probes has been observed experimentally. As a comparison, for **NI**, the maximum oscillator strength appears in $S_0 \longrightarrow S_1$ transition ($f = 0.200$), which is mainly contributed by the transition of HOMO to LUMO (Table S9). With both molecular orbitals settled on the **NI** moiety and no other state between S_0 and S_1 (LE state), its fluorescence shines out unrestrictedly (Figure 7(c), right), ensuring the excellent applications in bioimaging with **NI**-based probes. Taken together, the existence of a nitro group in the intact probe induces a d-PET process caging the fluorescence, avoiding a background noise arising from the probe itself.

3. Discussion

Finely turning down the nonenzymatic reactivity with GSH plays a pivotal role in reducing the background noise of a GST detection probe while maintaining a considerable sensitivity. We have adopted and established the local electrophilicity index ω_k as efficient to characterize this reactivity and thus developed a rational semiquantitative strategy to design a two-photon fluorescent probe for GSTs with high sensitivity and S/N ratio by evaluating its ω_k. In this way, **NI3** has been selected, and both examinations *in vitro* and bioimaging in live cells or tissue sections verify its outstanding performances, demonstrating the feasibility of this strategy. Moreover, besides the modestly lower ω_k, the success of achieving a low background noise depends on the caged fluorescence of intact probes by PET mechanism as well, which is observed for the first time by femtosecond TA spectra for **NI**-based probes, and a theoretical study based on TD-DFT calculations has explained how PET, and thus, fluorescence quenching happens.

In summary, this work highlights the start of introducing a parameter from CDFT to GST probe design. Theoretically speaking, the ω_k adopted here is not only limited to GST probe design but can be widely used for any probes based on S_NAr reactions between soft nucleophile and soft electrophile. Overall, we anticipate our strategy will inspire more high-performance probes like **NI3** to be applied to biomedical research in the future.

Data Availability

All data needed to evaluate the conclusions in the paper are present in the paper and/or the Supplementary Materials. Any additional datasets, analysis details, and material recipes are available upon request.

Conflicts of Interest

The authors declare no conflicts of interest.

Authors' Contributions

X. X. Zhang wrote the manuscript. H. Qi performed the biological experiments. X. X. Zhang and M. H. Lu conducted the computational work. S. Q. Yang and P. Li contributed materials/analysis tools. K. L. Han and H. L. Piao planned and initiated the project, designed experiments, and supervised the entire project. Xue-Xiang Zhang and Huan Qi contributed equally to this work.

Acknowledgments

This paper is dedicated to the 70th anniversary of the Dalian Institute of Chemical Physics, Chinese Academy of Sciences. The authors thank Pramod Pandey for meritorious suggestions on exploring the cause of problems in analytical chemistry, Han Liao for constructive advice on biochemistry, Run-Ze Liu for theoretical guidance, Qi-Chao Yao for preparation of tissue slices, Ning-Jiu Zhao for guidance on TA experiment, and Guang-Hua Ren for dedicated review of the manuscript. This work was supported by the Scientific Instrument Developing Project of the Chinese Academy of Sciences (Grant No. YJKYYQ20190003), the Liao Ning Revitalization Talents Program (XLYC1802126), the Dalian City Foundation for Science and Technology Innovation (2019J12GX031), and the National Natural Science Foundation of China (Grant Nos. 21673237 and 21503224).

Supplementary Materials

Detailed experimental and computational methods, material preparations, characterizations, fluorescence imaging videos, and supplementary figures and tables are available in Supplementary Materials. *(Supplementary Materials)*

References

[1] R. N. Armstrong, "Structure, catalytic mechanism, and evolution of the glutathione transferases," *Chemical Research in Toxicology*, vol. 10, no. 1, pp. 2–18, 1997.

[2] B. Mannervik, U. Helena Danielson, and B. Ketterer, "Glutathione transferases–structure and catalytic Activit," *Critical*

Reviews in Biochemistry and Molecular Biology, vol. 23, no. 3, pp. 283–337, 1988.

[3] W. Zhou, J. W. Shultz, N. Murphy et al., "Electrophilic aromatic substituted luciferins as bioluminescent probes for glutathione S-transferase assays," *Chemical Communications*, vol. 42, no. 44, pp. 4620–4622, 2006.

[4] J. D. Hayes and D. J. Pulford, "The Glut athione S-transferase supergene family: regulation of GST and the contribution of the lsoenzymes to cancer chemoprotection and drug resistance Part I," *Critical Reviews in Biochemistry and Molecular Biology*, vol. 30, no. 6, pp. 445–520, 1995.

[5] A. Bennaceur-Griscelli, J. Bosq, S. Koscielny et al., "High level of glutathione-S-transferase pi expression in mantle cell lymphomas," *Clinical Cancer Research*, vol. 10, no. 9, pp. 3029–3034, 2004.

[6] M. A. Harkey, M. Czerwinski, J. Slattery, and H. P. Kiem, "Overexpression of glutathione-S-transferase, MGSTII, confers resistance to busulfan and melphalan," *Cancer Investigation*, vol. 23, no. 1, pp. 19–25, 2005.

[7] J. D. Hayes, J. U. Flanagan, and I. R. Jowsey, "Glutathione transferases," *Annual Review of Pharmacology and Toxicology*, vol. 45, pp. 51–88, 2005.

[8] C. C. McIlwain, D. M. Townsend, and K. D. Tew, "Glutathione *S* -transferase polymorphisms: cancer incidence and therapy," *Oncogene*, vol. 25, no. 11, pp. 1639–1648, 2006.

[9] X. Wang, X. Y. Lou, X. Y. Jin, F. Liang, and Y. W. Yang, "A binary supramolecular assembly with intense fluorescence emission, high pH stability, and cation selectivity: supramolecular assembly-induced emission materials," *Research*, vol. 2019, article 1454562, 10 pages, 2019.

[10] E. J. Kim, R. Kumar, A. Sharma et al., "In vivo imaging of β-galactosidase stimulated activity in hepatocellular carcinoma using ligand-targeted fluorescent probe," *Biomaterials*, vol. 122, pp. 83–90, 2017.

[11] J. Bai, L. Zhang, H. Hou, Z. Shi, J. Yin, and X. Jiang, "Light-written reversible 3D fluorescence and topography dual-pattern with memory and self-healing abilities," *Research*, vol. 2019, article 2389254, 11 pages, 2019.

[12] J. Ning, T. Liu, P. Dong et al., "Molecular design strategy to construct the near-infrared fluorescent probe for selectively sensing human cytochrome P450 2J2," *Journal of the American Chemical Society*, vol. 141, no. 2, pp. 1126–1134, 2019.

[13] G. Jiang, G. Zeng, W. Zhu et al., "A selective and light-up fluorescent probe for β-galactosidase activity detection and imaging in living cells based on an AIE tetraphenylethylene derivative," *Chemical Communications*, vol. 53, no. 32, pp. 4505–4508, 2017.

[14] Y. Fujikawa, Y. Urano, T. Komatsu et al., "Design and synthesis of highly sensitive fluorogenic substrates for glutathione S-transferase and application for activity imaging in living cells," *Journal of the American Chemical Society*, vol. 130, no. 44, pp. 14533–14543, 2008.

[15] J. Zhang, A. Shibata, M. Ito et al., "Synthesis and characterization of a series of highly fluorogenic substrates for glutathione transferases, a general strategy," *Journal of the American Chemical Society*, vol. 133, no. 35, pp. 14109–14119, 2011.

[16] Y. Fujikawa, F. Morisaki, A. Ogura et al., "A practical fluorogenic substrate for high-throughput screening of glutathione S-transferase inhibitors," *Chemical Communications*, vol. 51, no. 57, pp. 11459–11462, 2015.

[17] J. Zhang, Z. Jin, X. X. Hu et al., "Efficient two-photon fluorescent probe for glutathione S-transferase detection and imaging in drug-induced liver injury sample," *Analytical Chemistry*, vol. 89, no. 15, pp. 8097–8103, 2017.

[18] W. Jiang, Q. Fu, H. Fan, J. Ho, and W. Wang, "A highly selective fluorescent probe for thiophenols," *Angewandte Chemie International Edition*, vol. 46, no. 44, pp. 8445–8448, 2007.

[19] J. Bouffard, Y. Kim, T. M. Swager, R. Weissleder, and S. A. Hilderbrand, "A highly selective fluorescent probe for thiol bioimaging," *Organic Letters*, vol. 10, no. 1, pp. 37–40, 2008.

[20] L. Yuan, W. Lin, S. Zhao et al., "A unique approach to development of near-infrared fluorescent sensors for in vivo imaging," *Journal of the American Chemical Society*, vol. 134, no. 32, pp. 13510–13523, 2012.

[21] X. Ji, R. N. Armstrong, and G. L. Gilliland, "Snapshots along the reaction coordinate of an SNAr reaction catalyzed by glutathione transferase," *Biochemistry*, vol. 32, no. 48, pp. 12949–12954, 1993.

[22] L. R. Domingo, P. Perez, and J. A. Saez, "Understanding the local reactivity in polar organic reactions through electrophilic and nucleophilic Parr functions," *RSC Advances*, vol. 3, no. 5, pp. 1486–1494, 2013.

[23] L. R. Domingo, P. Perez, M. J. Aurell, and J. A. Saez, "Understanding the bond formation in hetero-Diels-Alder reactions. An ELF analysis of the reaction of nitroethylene with dimethylvinylamine," *Current Organic Chemistry*, vol. 16, no. 19, pp. 2343–2351, 2012.

[24] L. R. Domingo, P. Perez, and J. A. Saez, "Origin of the synchronicity in bond formation in polar Diels-Alder reactions: an ELF analysis of the reaction between cyclopentadiene and tetracyanoethylene," *Organic & Biomolecular Chemistry*, vol. 10, no. 19, pp. 3841–3851, 2012.

[25] L. R. Domingo, P. Perez, and J. A. Saez, "Understanding the regioselectivity in hetero Diels-Alder reactions. An ELF analysis of the reaction between nitrosoethylene and 1-vinylpyrrolidine," *Tetrahedron*, vol. 69, no. 1, pp. 107–114, 2013.

[26] A. T. Maynard, M. Huang, W. G. Rice, and D. G. Covell, "Reactivity of the HIV-1 nucleocapsid protein p7 zinc finger domains from the perspective of density-functional theory," *Proceedings of the National Academy of Sciences of the United States of America*, vol. 95, no. 20, pp. 11578–11583, 1998.

[27] R. G. Parr, L. Von Szentpaly, and S. Liu, "Electrophilicity index," *Journal of the American Chemical Society*, vol. 121, no. 9, pp. 1922–1924, 1999.

[28] I. M. C. M. Rietjens, A. E. M. F. Soffers, G. J. E. J. Hooiveld, C. Veeger, and J. Vervoort, "Quantitative structure-activity-relationships based on computer calculated parameters for the overall rate of glutathione-S-transferase catalyzed conjugation of a series of fluoronitrobenzenes," *Chemical Research in Toxicology*, vol. 8, no. 4, pp. 481–488, 1995.

[29] P. K. Chattaraj, *Chemical Reactivity Theory: A Density Functional View. Ch. 18*, CRC Press, Boca Raton, 2009.

[30] G. Klopman, "Chemical reactivity and the concept of charge- and frontier-controlled reactions," *Journal of the American Chemical Society*, vol. 90, no. 2, pp. 223–234, 1968.

[31] X. X. Zhang, H. Wu, P. Li, Z. J. Qu, M. Q. Tan, and K. L. Han, "A versatile two-photon fluorescent probe for ratiometric imaging E. coli β-galactosidase in live cells and in vivo," *Chemical Communications*, vol. 52, no. 53, pp. 8283–8286, 2016.

[32] H. W. Liu, S. Xu, P. Wang et al., "An efficient two-photon fluorescent probe for monitoring mitochondrial singlet oxygen in

tissues during photodynamic therapy," *Chemical Communications*, vol. 52, no. 83, pp. 12330–12333, 2016.

[33] M. Torrent-Sucarrat, M. Duran, and M. Sola, "Global hardness evaluation using simplified models for the hardness kernel," *The Journal of Physical Chemistry A*, vol. 106, no. 18, pp. 4632–4638, 2002.

[34] M. Torrent-Sucarrat, J. M. Luis, M. Duran, A. Toro-Labbe, and M. Sola, "Relations among several nuclear and electronic density functional reactivity indexes," *The Journal of Chemical Physics*, vol. 119, no. 18, pp. 9393–9400, 2003.

[35] R. K. Roy, K. Hirao, and S. Pal, "On non-negativity of Fukui function indices. II," *The Journal of Chemical Physics*, vol. 113, no. 4, pp. 1372–1379, 2000.

[36] R. K. Roy, K. Hirao, S. Krishnamurty, and S. Pal, "Mulliken population analysis based evaluation of condensed Fukui function indices using fractional molecular charge," *The Journal of Chemical Physics*, vol. 115, no. 7, pp. 2901–2907, 2001.

[37] J. H. T. M. Ploemen, B. van Ommen, J. J. P. Bogaards, and P. J. van Bladeren, "Ethacrynic acid and its glutathione conjugate as inhibitors of glutathione *S*-transferases," *Xenobiotica*, vol. 23, no. 8, pp. 913–923, 1993.

[38] J. Hansson, K. Berhane, V. M. Castro, U. Jungnelius, B. Mannervik, and U. Ringborg, "Sensitization of human melanoma cells to the cytotoxic effect of melphalan by the glutathione transferase inhibitor ethacrynic acid," *Cancer Research*, vol. 51, no. 1, pp. 94–98, 1991.

[39] J. A. Moscow, C. R. Fairchild, M. J. Madden et al., "Expression of anionic glutathione-S-transferase and P-glycoprotein genes in human tissues and tumors," *Cancer Research*, vol. 49, no. 6, pp. 1422–1428, 1989.